Surfaces and Interfaces 25 (2021) 101151

Contents lists available at ScienceDirect

Surfaces and Interfaces

journal homepage: www.sciencedirect.com/journal/surfaces-and-interfaces

Synthesis of Ag-embedded SnS films by the RF method for photovoltaic applications

Tien Dai Nguyen [a,b,*], Van Thai Dang [a,c], Nguyen Manh Hung [d,**], Vinaya Kumar Arepalli [e], Jeha Kim [e], Marnadu Raj [f], Thi Tu Oanh Nguyen [g]

[a] Institute of Theoretical and Applied Research, Duy Tan University, Hanoi 100000, Vietnam
[b] Faculty of Natural Science, Duy Tan University, Da Nang 550000, Vietnam
[c] Faculty of Environmental and Chemical Engineering, Duy Tan University, Da Nang 550000, Vietnam
[d] Department of Materials Science and Engineering, Le Quy Don Technical University, Hanoi 100000, Vietnam
[e] Department of Energy Convergence Engineering, Cheongju University, Cheongju 28503, Republic of Korea
[f] Department of Physics, Sri Ramakrishna Mission Vidyalaya College of Arts and Science, Coimbatore 641 020, Tamil Nadu, India
[g] Institute of Materials Science, Vietnam Academy of Science and Technology, 18 Hoang Quoc Viet, Cau Giay, Hanoi, Vietnam

ARTICLE INFO

Keywords:
SnS
Ag
RF sputtering method
Photovoltaic

ABSTRACT

In this study, we report on the synthesis of SnS/Ag/SnS trilayer films for photovoltaic applications by the radio frequency (RF) sputtering method. The effect of the Ag thin film on the physical properties of the SnS film was systematically investigated. The SnS/Ag/SnS trilayer film solar cell obtained a higher short circuit current density (J_{sc}) of 17.13 mA/cm^2 and a higher efficiency (η_{max}) of 5.24% than those of the SnS film solar cell (J_{sc} = 14.21 mA/cm^2, η = 3.23%). The improved photocurrent density (PCD) mainly resulted from the enhancement of the separation efficiency of photogenerated electron-hole pair and the decrease in trapping charge carriers in impurity centers as well as the reduction of the leakage current in the active region. These results could be useful for fabricating the next-generation photovoltaic device with high efficiency.

1. Introduction

In recent years, quasi–two dimensional (2D) tin (II) monosulphide (SnS) has been received much attention for optoelectronic applications (photovoltaic [1–6], photodetector [7–9], hydrogen evolution [10–12]) because of the advantages of the high absorption efficiency [13] (10^4–10^5 cm^{-1}), the maximum theoretical conversion efficiency (16–25.268%) [3,14], the excellent sensing performance [9] (3.3×10^{12} Jones) and the eco-friendly device fabrication. The SnS has shown p−type semiconductor property (tunable bandgap 1.08–1.7 eV), high carrier concentration (6.95×10^{15} cm^{-3}) and large−scale power generation, thermal stability [1,5,7,9,15–19]. Besides that, the intrinsic SnS film is a promising candidate for photovoltaic application due to its high conversion efficiency of 4.36% [20,5], slow charge recombination, and large absorption coefficient (1.1×10^5 cm^{-1}) [1]. To date, the SnS film has been synthesized via many approaches (chemical vapor deposition [21,9], sputtering [1,22], atomic layer deposition [17], electrochemical [23], chemical bath deposition [24], e−beam evaporation [25], thermal evaporation [6] and spray pyrolysis [26]). However, most studies indicated that the optical efficiency of the SnS compound has been lower than the theoretical efficiency of 32% due to the existent limitation [27,28,19]. Many works have done to improve the conversion efficiency of the SnS based photovoltaic device from 1.33 to 4.63% [4–6]. Besides that, the metal-doped SnS has showed the enhancement of its electrical and optical properties [29–31,2,32–35]. Among the metal dopants, silver is a potential candidate for doping SnS thin film due to the suitable ionic radii of dopant cation Ag^{2+} (106 pm) as compared to that of ion Sn^{2+}(118 pm) [36,37]. Several reports of as-synthesized Ag-doped SnS film showed a large absorption coefficient, high carrier mobility, low resistivity (3.1 Ω) [37], and enhanced charge collection [38,29,30,2,37]. In addion, due to the surface plasmon resonance effect the photovoltaic cells with loading noble metal nanoparticle (Pt, Au, Ag) have been shown enhancing electrical and optical properties, which improves efficiency with plasmonic behavior [39–43]. Recently, Cho et al. [20] have developed and improved the performance of SnS/CdS solar cells by vapor transport deposition method. Interestingly, they noted that the

* Corresponding author at: Institute of Theoretical and Applied Research, Duy Tan University, Hanoi 100000, Vietnam.
** Co-corresponding author.
E-mail addresses: nguyentiendai@duytan.edu.vn (T.D. Nguyen), hungnm@lqdtu.edu.vn (N.M. Hung).

https://doi.org/10.1016/j.surfin.2021.101151
Received 4 March 2021; Received in revised form 9 April 2021; Accepted 16 April 2021
Available online 29 April 2021

SnS based cell performance was strongly influenced by the interface quality. Yun et al [44] have reported efficient nanostructured TiO_2/SnS heterojunction solar cells on FTO substrate using the spin coating method. They improved the performance of the devices and achieved the highest PCE of ≈ 4.8% due to the formation of a more uniform and denser layer. Nicolae Spalatu et al. [45] fabricated FTO/CdS/SnS structure solar cell and studied the effect of annealing temperature on the device performance. They demonstrated that SnS films with large, sintered, and doped grains are the potential for enhancement of the SnS device efficiency. Interestingly, the band discontinuities in the conduction band of SnS might manipulate band gap and band positions, which reduces the negativity of the conduction band discontinuity and turn it into a positivity [30,2,33,35]. These useful physical properties causes it a candidate for optoelectronic devices. However, the effect of Ag-doped SnS nanofilms on photovoltaic performance has not been studied clearly so far. Continuing our previous studies, [38,46] we synthesized the active layer of SnS/Ag/SnS trilayer structure by the radio frequency (RF) sputtering method. Loading of an Ag thin film, the effect of Ag on the structural, morphological, electrical and optical properties of the SnS film were investigated. The prepared SnS/Ag/SnS trilayer was used as an active layer for the fabrication of high performance solar cell, studying a potential photovoltaic application. Also, the characteristic performance of the configured device was studied.

2. Experimental

The trilayer film of SnS/Ag/SnS structure was deposited on both the soda-lime glass (SLG) and indium–dope tin oxide (ITO, Sigma Aldrich, 8 Ω/sq, 200 nm thick) substrates using the radio frequency (RF) sputtering method [38, 46]. The SnS (99.99%), Ag (99.999%) and TiO_2 (99.9%) targets (from MIT Corporation) were used for the deposition of thin films. Acetone (CH_3COCH_3, 99.5%) and alcohol (CH_3CH_2OH, 95%) were bought from Sigma Aldrich.

Firstly, the substrates were ultrasonically and sequentially cleaned with ethanol, acetone, and deionized water (DI) water for 10 min and then dried with N_2 (99.9%) gas. We used the active layer of SnS/Ag/SnS trilayer structure on the ITO substrate to fabricate the high performance solar cell device. The solar cell consisted of a 300 nm p^+–SnS (1×10^{18} cm^{-3}) blocking layer, an active layer of (1 μm thick SnS (1×10^{15} cm^{-3}), 5 nm thick Ag, and 1 μm thick SnS (1×10^{15} cm^{-3}), and a 500 nm thick n^+–SnS (1×10^{18} cm^{-3}) top layer). Then, a 100 nm thickness of TiO_2 layer was deposited on n^+–SnS for protecting and preventing the reaction of oxygen and Sn/S to form native oxides. Each layer was synthesized by the RF method (80 W of power, 3×10^{-3} torr of working pressure, 10 cm of distance, at 350 °C) [4]. The samples were named by DS01-05 with detailed structure, respectively, in Table 1. The metal contact layer of Pd/Ge/Au/Ti/Au (5/30/15/30/250 nm) was deposited by the electron beam evaporation and then annealing at 200 °C for enhancing ohmic contact.

The structure, morphology, and elemental concentration of samples were investigated by the Rigaku equipment (JD2584N, Cu_K_α radiation, λ = 1.54 Å) field emission scanning electron microscope (FE–SEM, Hitachi S4800) and energy–dispersive X−ray spectroscopy (EDS) technique (JED–2300 Analys Station equipment). The optical properties were characterized by the ANDOR spectroscopy (using 532–nm of excited wavelength), and the UV–2600 spectrophotometer. Characterizations of the solar cell were done by using the solar simulation system (PEC–L01, AM 1.5G, lamp power 150 mW.cm^{-2} (Serial. No. 1750163), on the active area of 0.616 cm^2.

3. Results and discussion

Fig. 1(a) presents the XRD patterns of SnS (DS02 sample) and Ag/SnS films (DS03 sample). As a result, the XRD peaks at 2θ = 21.98, 26.03, 27.35, 30.48, 31.59, 39.13, 44.83, 48.69, 51.28, 53.21, 64.18, and 66.76° correspond to the atomic planes of (0 1 1), (0 1 2), (0 2 1), (1 1 0), (0 1 3), (1 0 4), (0 2 2), (0 0 6), (1 1 5), (2 1 2), (1 2 5) and (0 0 8) of the SnS, respectively (JCPDS No.001–0984). The other peaks at 2θ = 38.08 and 44.25° that are assigned to the atomic planes of (1 1 1) and (2 0 0) of Ag phase, according to JCPDS No. 04–0783. These phases confirmthe presence of Ag thin film on SnS. The reduction of peak intensity (at 44.83°) and phase absence (at 27.51, 42.61, and 75.37°) are due to the effect of silver film and a dominating orientation during the sputtering process at temperature of 350 °C. We also obtained some unidentified peaks in the XRD pattern that are probably some other polymorphs from the Sn−S system during the sputtering process. However, the Ag/SnS film is still observed at the same peak positions as the orthorhombic phase of the SnS compound [47,29,30,15,2,48].

Fig. 1(b) exhibits the energy-dispersive X-ray spectroscopy (EDS) result of bare Ag/SnS thin film (DS03 sample). As can be seen from the figure, tin, sulfur, and silver made up 49.5%, 49.1% (Sn/S ratio is approximately of 1:1), and 1.05% in weight, respectively. Besides that, the EDS indicated 0.35% of the oxygen element that originally came from native oxide of the surface and the residual oxygen gas when the sample was processed in air. The residual oxygen might react with Sn and S to form S_7O_2, S_6O_2, SO_2, SO, SnO_2 and SnO alloys that affect the amorphous structure and carrier mobility of the SnS film. Thus, device performance might be affected by this issue. For reducing oxygen elements from residual oxygen gas, the surface sample needs to be pretreated (dry etching) at a high vacuum ($>10^{-11}$ Tor).

Fig. 2 presents the morphology of SnS (DS02 sample), and Ag/SnS thin films (DS03 sample), which were deposited at a substrate temperature of 350 °C by the RF sputtering method. As seen in Fig 2(a), samples showed a smooth surface of quasi-2 dimensional (2D) . This layer also shows low porosity, which is suitable for device fabrication. In Fig. 2(b), the Ag thin film on the SnS surface can not be observed via FE-SEM image due to the small silver amount (5 nm thick). However, the SEM image of Ag/SnS film of the improved conductivityhas a brighter color comparing to Fig 2(a).

Raman spectra of SnS (DS02 sample) and Ag/SnS (DS03 sample) films are shown in Fig. 3(a). They showed $2B_{3g}$ modes at 49.2, 162.1 cm^{-1}, $3A_g$ modes at 94.2, 223.5, 277.2 cm^{-1}, and $2B_{2g}$ modes at 170.5,

Table 1
Synthesis conditions of SnS and Ag/SnS thin film and their characteristics.

Samples	Structure	RF Sputtering condition					Optical Characteristics			Photovoltaics Characteristics			
		Substrate Temp. (°C)	Power (W)	Working pressure (mTorr)	Deposition time (min)	Ag thickness (nm)	$E_{absorp.}$ (eV)	$PL_{emi.}$ (eV)	Raman (cm^{-1})	J_{SC} (mA/cm^2)	V_{OC} (V)	FF	η (%)
DS01	SnS/ITO	350	80	30	5	–	–	–	–	–	–	–	–
DS02	SnS/ITO	350	80	30	70	–	1.55	1.46	×	–	–	–	–
DS03	Ag/SnS/ITO	350	80	30	71	5	1.53	1.46	×	–	–	–	–
DS04	TiO_2/*n*-SnS/SnS/*p*-SnS/ITO	350	80	30	70	–	–	–	–	14.21	0.42	0.54	3.23
DS05	TiO_2/*n*-SnS/SnS/Ag/SnS/*p*-SnS/ITO	350	80	30	70	5	–	–	–	17.13	0.45	0.68	5.24

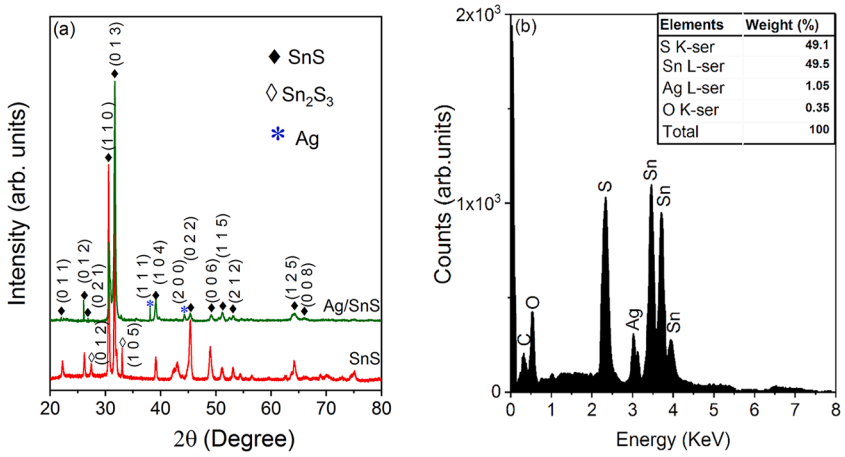

Fig. 1. (a) XRD patterns of SnS and Ag/SnS films as-deposited at 350 °C for DS02 and DS03 samples, respectively, and (b) EDS results of Ag/SnS film (DS03 sample).

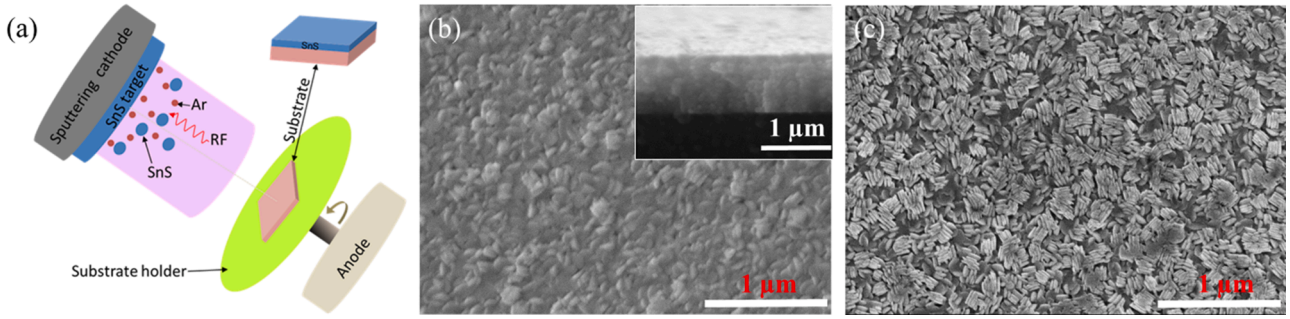

Fig. 2. The SEM images of (a) SnS film (DS02 sample), and (b) Ag/SnS film (DS03 sample).

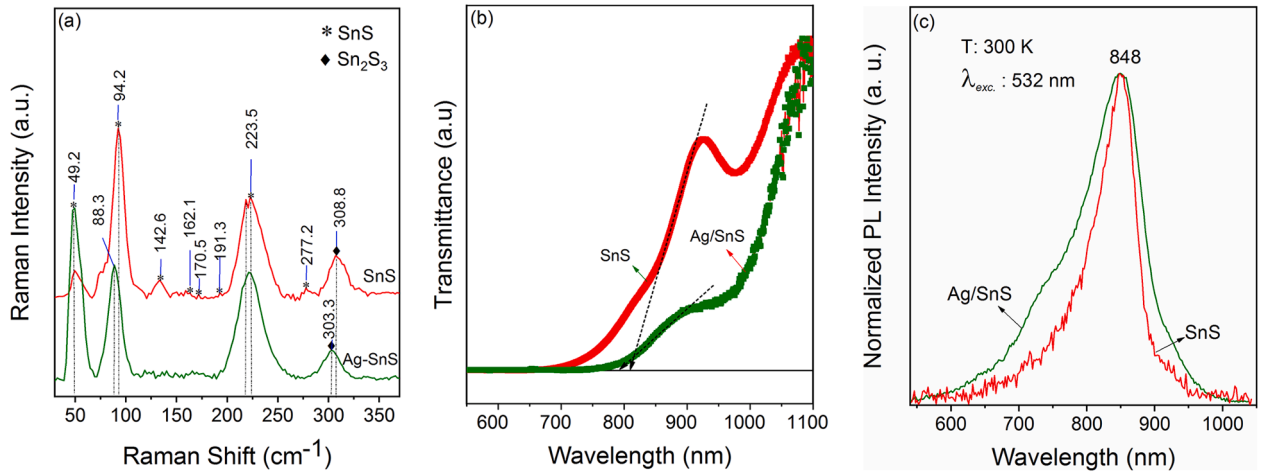

Fig. 3. Optical properties of SnS film (DS02 sample) and Ag/SnS film (DS03 sample) at room temperature: (a) Raman spectra, (b) Spectral transmittance, and (c) Spectral photoluminescence.

191.3 cm^{-1} of the SnS phase [49]. The mode at 308.8 cm^{-1} was attributed to the Sn_2S_3, this and the SnS peaks together indicated the mixing of SnS and Sn_2S_3 phases at high temperature [1, 50, 51]. The formation mechanism of the Sn_2S_3 phase has not been understood clearly, which needs to study further. In addition, the vibrational mode at 142.6 cm^{-1} (B_{2u}) is infrared active. The vibrational frequencies of the Ag/SnS film sample were shifted towards lower wavenumbers than these of the SnS film due to the Ag–Sn–S bond of the orthorhombic phase of the SnS compound. However, Ag/SnS thin film still observes the main peaks from the oscillation of the compound lattice. Interestingly, the intensity of B_{3g} mode (at 49.2 cm^{-1}) of Ag/SnS sample is higher than that of the SnS sample, which is attributed to the surface enhanced resonant Raman scattering (SERRS) due to small Ag nanoparticle size on SnS surface [52, 43]. This phenomenon might improve optoelectronics performance when the Ag/SnS film is used for device fabricating.

Fig. 3(b-c) shows the spectral transmittance and photoluminescence (PL) of SnS (DS02 sample), and Ag/SnS (DS03 sample) thin films at room temperature. The spectral transmittance of films exhibited direct bandgap behavior (E_g = 1.2–1.8 eV), which matched well with the previous reports [38,1,53,22,46,18]. Fig. 3(b) obtained a peak at 928

nm (1.36 eV) of both samples, which was attributed to the phase change in the optical absorption edge due to the presence of both the Sn_2S_3 [21] compound and tin oxide (SnO_2) [18]. The E_g of the DS03 sample was lower (80 me*V*) than that of SnS film. However, the PL peaks of them were observed at the same position 848 nm ($E_g = 1.46$ e*V*) with the full with half maximum (FWHM) of 263, and 169 me*V* for SnS and Ag/SnS film, respectively, as shown in Fig. 3 (c). The FWHM of the DS03 sample is larger than that of the DS02 sample. This might be attributed to the center Sn_2S_3 impurities or other polymorphs in the Sn-S system, and and polytytic hybrid nanocrystal (SnS−Sn_2S_3, and SnS−Sn_2S_3−SnS_2, SnS−SnS_2, Sn_2S_3−SnS_2) [54]. Also, the deposition of Ag film on the SnS may form amorphous phases of Ag-S alloy and large Ag particles on SnS film. These reasons cause reducing intensity and broadern peak of spectral photoluminescence of Ag/SnS film. This asymmetric broad peak phenomenon was not well understood, thus we will study further in the future.

Fig. 4(a) shows the current−voltage curves (*J*−*V*) of the DS05 sample measured in a dark condition for the rapid thermal annealing (RTA), and without RTA condition. The inserted picture of Fig. 4(a) indicates the schematic structure of the photovoltaic device with precise thickness and concentration. The linear slope of the *J*−*V* curves indicated that an ohmic contact have been successfully built between the metal layers of Pd/Ge/Au/Ti/Au and SnS film. The current density abruptly increases after the RTA with an open-circuit voltage of 0.45 *V*. In Fig. 4(b), the *J*–*V* curve characteristics of SnS/Ag/SnS trilayer and SnS film solar cells were measured at room temperature. The fill factor (*FF*), short circuit current density (J_{SC}), open-circuit voltage (V_{OC}) and power conversion efficiency (η) of the solar cell are evaluated from the above *J*–*V* curves, as listed in Table 1. As a result, the J_{SC} (17.13 mA/cm^2) of the DS05 sample is higher than that of SnS (14.21 mA/cm^2) film (DS04 sample). Especially, our device obtained the power conversion efficiency of 5.24% (fill factor of 0.68), which is higher than that of previous reports (3.88–4.36%) [55,56,5,57,6], as listed in Table 2. The reason was the higher separation, less recombination of photogenerated carriers and low carrier recombination density. Morover, due to the surface plasmonic resonance effect of Ag nanoparticles sandwiched between two SnS layers, the light absorption efficiency is improved [58,59], leading to more charge carriers being generated. The energy bandgap of TiO_2 (3.2 eV) is higher than that of SnS (1.12–1.5 eV) layer, which is a band filter for light absorption. Also, the reverse injection of non-desired carriers might be blocked by the TiO_2 layer when they are generated at electrodes, which improves the power conversion efficiency of the device. On the other hand, the high power conversion efficiency resulted from the high fill factor (FF) and the low series resistance (R_s) [60,61]. The shunt resistance due to the leak current between the layers (SnS–Ag–SnS, SnS–TiO_2) affected the FF of the device. Thus, we should reduce the defect of layers and enhance the ohmic contact (Pd/Ge/Au/Ti/Au) layers by using a substrate temperature of 350 °C for depositing film and the RTA technique at 200 °C. The evaluated value of the series resistance from the above *J*-*V* curve (DS05 sample) was approximately 16.2 Ω. However, this value is still high, leading to reduce the photocurrent density of the out circuit. The Ag particles between both SnS films are large (ac. 2–5 nm) that might cause reduced photo conversion efficiency due to internal leak current. Thus, we further need to reduce these issues via Ag−doping SnS film that affect the series resistance and leak current for improving the conversion efficiency of the SnS solar cell.

Table 2
Comparison of photovoltaic characteristics of SnS-base solar cells

Structure	Photovoltaics Characteristics				References
	J_{SC} (mA/cm^2)	V_{OC} (*V*)	FF	η (%)	
TiO_2/*n*-SnS/SnS/Ag/SnS/*p*-SnS/ITO	17.13	0.45	0.68	5.24	This work
Mo/SnS/SnO_2/*n*-ZnO/ITO	20.2	0.37	0.58	4.36	[46]
Al/ITO/i-ZnO/CdS/SnS/Mo/SLG	10.28	0.141	0.399	0.58	[44]
Si/SiO_2/Mo/SnS/Zn(O,S):N/ZnO/ITO/Ag	20.645	0.344	0.56	3.88	[1]
Mo/SnS/ZnMgO/ZnO:Al/Ag	9.96	0.575	0.364	2.02	[45]
FTO/TiO_2/SnS/P_3HT/Ag	7.35	0.85	0.45	2.81	[46]
p-SnS/*n*-CdS	9.6	0.26	0.53	1.3	[4]
ZnS/SnS	31.88	0.894	0.57	16.26	[14] Simulation
n-SnS/*p*-SnS	29.313	0.985	0.876	25.268	[3] Simulation

4. Conclusion

SnS/Ag/SnS trilayer film was synthesized successfully on the ITO substrate by the radio frequency (RF) sputtering approach. Ag film with a 5 nm thickness was deposited on the SnS film at a temperature of 350 °C to enhance photovoltaic capability. The Ag/SnS film showed a *p*-type semiconducting behavior with the bandgap via the optical absorption edge at 809 nm and a strong PL peak at 848 nm (1.46 eV). From the *I*-*V* results, we observed that the SnS/Ag/SnS trilayer film based solar cell achieved higher values of $J_{SC} = 17.13$ mA/cm^2, $V_{op} = 0.45$ V and $\eta = 5.24\%$ at room temperature. Noted that it was better than SnS film-based solar cell due to the higher separation, lesser recombination of light generated carriers, low carrier recombination density, the low

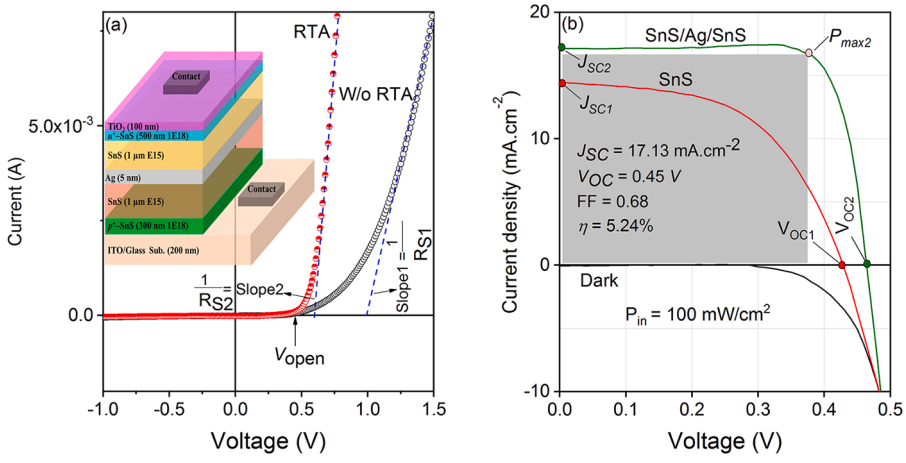

Fig. 4. (a) The dark- and (b) irradiated−forward *J*-*V* characteristics of solar cells made from the SnS film (DS04 sample) and SnS/Ag/SnS film (DS05 sample).

defect density and effect plasmonic of Ag on the active layer. As a result, it is a potential approach to improve the photon conversion efficiency of the SnS solar cell using noble metals for the photovoltaic device.

Declaration of Competing Interest

None.

Acknowledgments

This research is supported by Vietnam National Foundation for Science and Technology Development (NAFOSTED) under grant number 9/2020/STS02, and authors are thankful to Dr. Sang Jun Lee (KRISS) for solar cell measurements.

Reference

[1] V.K. Arepalli, Y. Shin, J. Kim, Influence of working pressure on the structural, optical, and electrical properties of RF-sputtered SnS thin films, Superlattices Microst. 122 (2018) 253–261.
[2] S. Gedi, V.R. Minnam Reddy, T.R. Reddy Kotte, S.-H. Kim, C.-W. Jeon, Chemically synthesized Ag-doped SnS films for PV applications, Ceram. Int. 42 (16) (2016) 19027–19035.
[3] S. Lin, X. Li, H. Pan, H. Chen, X. Li, Y. Li, J. Zhou, Numerical analysis of SnS homojunction solar cell, Superlattices and Microstruct 91 (2016) 375–382.
[4] K.T. Ramakrishna Reddy, N.K. Reddy, R.W. Miles, Photovoltaic properties of SnS based solar cells, Sol. Energy Mater. Sol. Cells 90 (18) (2006) 3041–3046.
[5] P. Sinsermsuksakul, L. Sun, S.W. Lee, H.H. Park, S.B. Kim, C. Yang, R.G. Gordon, Overcoming efficiency limitations of SnS-based solar cells, Adv. Energy Mater. 4 (15) (2014), 1400496.
[6] V. Steinmann, R. Jaramillo, K. Hartman, R. Chakraborty, R.E. Brandt, J. R. Poindexter, Y.S. Lee, L. Sun, A. Polizzotti, H.H. Park, R.G. Gordon, T. Buonassisi, 3.88% Efficient tin sulfide solar cells using congruent thermal evaporation, Adv. Mater. 26 (44) (2014) 7488–7492.
[7] M.S. Mahdi, N.M. Ahmed, A. Hmood, K. Ibrahim, M. Bououdina, Comprehensive photoresponse study on high performance and flexible π-SnS photodetector with near-infrared response, Mater. Sci. Semicond. Process. 100 (2019) 270–274.
[8] M. Patel, M. Kumar, J. Kim, Y.K. Kim, Photocurrent enhancement by a rapid thermal treatment of nanodisk-shaped SnS photocathodes, J. Phys. Chem. Lett. 8 (24) (2017) 6099–6105.
[9] D. Zheng, H. Fang, M. Long, F. Wu, P. Wang, F. Gong, X. Wu, J.C. Ho, L. Liao, W. Hu, High-performance near-infrared photodetectors based on p-type SnX (X = S, Se) nanowires grown via chemical vapor deposition, ACS Nano 12 (7) (2018) 7239–7245.
[10] W. Cheng, N. Singh, W. Elliott, J. Lee, A. Rassoolkhani, X. Jin, E.W. McFarland, S. Mubeen, Earth-abundant tin sulfide-based photocathodes for solar hydrogen production, Adv. Sci. 5 (1) (2018), 1700362.
[11] W. Gao, C. Wu, M. Cao, J. Huang, L. Wang, Y. Shen, Thickness tunable SnS nanosheets for photoelectrochemical water splitting, J. Alloy. Compound. 688 (2016) 668–674.
[12] J.J.M. Vequizo, M. Yokoyama, M. Ichimura, A. Yamakata, Enhancement of photoelectrochemical activity of SnS thin-film photoelectrodes using TiO_2, Nb_2O_5, and Ta_2O_5 metal oxide layers, Appl. Phys. Express 9 (6) (2016), 067101.
[13] N. Koteeswara Reddy, K. Ramesh, R. Ganesan, K.T. Ramakrishna Reddy, K. R. Gunasekhar, E.S.R. Gopal, Synthesis and characterisation of co-evaporated tin sulphide thin films, Appl. Phys. A 83 (1) (2006) 133–138.
[14] J. Xu, Y. Yang, Study on the performances of SnS heterojunctions by numerical analysis, Energy Conv. Manag. 78 (2014) 260–265.
[15] L.A. Burton, D. Colombara, R.D. Abellon, F.C. Grozema, L.M. Peter, T.J. Savenije, G. Dennler, A. Walsh, Synthesis, characterization, and electronic structure of single-crystal SnS, Sn_2S_3, and SnS_2, Chem. Mater. 25 (24) (2013) 4908–4916.
[16] M. Devika, N.K. Reddy, K. Ramesh, R. Ganesan, K.R. Gunasekhar, E.S.R. Gopal, K. T.R. Reddy, Thickness effect on the physical properties of evaporated SnS films, J. Electrochem. Soc. 154 (2) (2007) H67–H73.
[17] G. Ham, S. Shin, J. Park, H. Choi, J. Kim, Y.-A. Lee, H. Seo, H. Jeon, Tuning the electronic structure of tin sulfides grown by atomic layer deposition, ACS Appl. Mater. Interfaces 5 (18) (2013) 8889–8896.
[18] O.E. Ogah, G. Zoppi, I. Forbes, R.W. Miles, Thin films of tin sulphide for use in thin film solar cell devices, Thin Solid Films 517 (7) (2009) 2485–2488.
[19] W. Shockley, H.J. Queisser, Detailed balance limit of efficiency of p-n junction solar cells, J. Appl. Phys. 32 (3) (1961) 510–519.
[20] J.Y. Cho, S. Kim, R. Nandi, J. Jang, H.-S. Yun, E. Enkhbayar, J.H. Kim, D.-K. Lee, C.-H. Chung, J. Kim, J. Heo, Achieving over 4% efficiency for SnS/CdS thin-film solar cells by improving the heterojunction interface quality, J. Mater. Chem. A 8 (39) (2020) 20658–20665.
[21] P. Kevin, D.J. Lewis, J. Raftery, M.Azad Malik, P. O'Brien, Thin films of tin(II) sulphide (SnS) by aerosol-assisted chemical vapour deposition (AACVD) using tin (II) dithiocarbamates as single-source precursors, J. Cryst. Growth 415 (2015) 93–99.
[22] K. Hartman, J.L. Johnson, M.I. Bertoni, D. Recht, M.J. Aziz, M.A. Scarpulla, T. Buonassisi, SnS thin-films by RF sputtering at room temperature, Thin Solid Films 519 (21) (2011) 7421–7424.
[23] A. Burgos, F. Cataño, B. Marí, R. Schrebler, H. Gómez, Pulsed electrodeposition of tin sulfide thin films from dimethyl sulfoxide solutions, J. Electrochem. Soc. 163 (9) (2016) D562–D567.
[24] M. Ichimura, K. Takeuchi, Y. Ono, E. Arai, Electrochemical deposition of SnS thin films, Thin Solid Films 361–362 (2000) 98–101.
[25] A. Tanuševski, D. Poelman, Optical and photoconductive properties of SnS thin films prepared by electron beam evaporation, Sol. Energy Mater. Sol. Cells 80 (3) (2003) 297–303.
[26] N. Koteswara Reddy, K.T.Ramakrishna Reddy, Growth of polycrystalline SnS films by spray pyrolysis, Thin Solid Films 325 (1) (1998) 4–6.
[27] C.H. Henry, Limiting efficiencies of ideal single and multiple energy gap terrestrial solar cells, J. Appl. Phys. 51 (8) (1980) 4494–4500.
[28] F. Meillaud, A. Shah, C. Droz, E. Vallat-Sauvain, C. Miazza, Efficiency limits for single-junction and tandem solar cells, Sol. Energy Mater. Sol. Cells 90 (18) (2006) 2952–2959.
[29] B.H. Baby, D. Bharathi Mohan, Characterization studies of heavily doped Ag-SnS thin films prepared by magnetron co-sputtering technique, Mater. Today-Proc. (2019).
[30] B.H. Baby, D. Bharathi Mohan, Structural, optical and electrical studies of DC-RF magnetron co-sputtered Cu, In & Ag doped SnS thin films for photovoltaic applications, Sol. Energy 194 (2019) 61–73.
[31] P.R. Bommireddy, C.S. Musalikunta, C. Uppala, S.-H. Park, Influence of Cu doping on physical properties of sol-gel processed SnS thin films, Mater. Sci. Semicond. Process 71 (2017) 139–144.
[32] H. Kafashan, Z. Balak, Preparation and characterization of electrodeposited SnS:In thin films: effect of In dopant, Spectroc. Acta Pt. A-Molec. Biomolec. Spectr. 184 (2017) 151–162.
[33] H. Kafashan, R. Ebrahimi-Kahrizsangi, F. Jamali-Sheini, R. Yousefi, Effect of Al doping on the structural and optical properties of electrodeposited SnS thin films, Phys. Status Solidi A-Appl. Mat. 213 (5) (2016) 1302–1308.
[34] A.G. Manohari, S. Dhanapandian, C. Manoharan, K.S. Kumar, T. Mahalingam, Effect of doping concentration on the properties of bismuth doped tin sulfide thin films prepared by spray pyrolysis, Mater. Sci. Semicond. Process 17 (2014) 138–142.
[35] M. Patel, A. Ray, Magnetron sputtered Cu doped SnS thin films for improved photoelectrochemical and heterojunction solar cells, RSC Adv 4 (74) (2014) 39343–39350.
[36] M. Devika, N.K. Reddy, K. Ramesh, K.R. Gunasekhar, E.S.R. Gopal, K.T.R. Reddy, Low resistive micrometer-thick SnS:Ag films for optoelectronic applications, J. Electrochem. Soc. 153 (8) (2006) G727.
[37] H.J. Jia, S.Y. Cheng, P.M. Lu, Effect of anneal time on photoelectric properties of SnS:Ag thin films, Adv. Mater. Res. 152–153 (2011) 752–755.
[38] V.K. Arepalli, T.D. Nguyen, J. Kim, Influence of Ag thickness on the structural, optical, and electrical properties of the SnS/Ag/SnS trilayer films for solar cell application, Curr. Appl. Phys. 20 (3) (2020) 438–444.
[39] S. Li, J. Hu, Y. Yang, L. Zhao, Y. Qiao, W. Liu, P. Liu, M. Chen, Ag/nano-TiO_2 composite compact film for enhanced performance of perovskite solar cells based on carbon counter electrodes, Appl. Phys. A 123 (10) (2017) 628.
[40] Y.-H. Su, Y.-F. Ke, S.-L. Cai, Q.-Y. Yao, Surface plasmon resonance of layer-by-layer gold nanoparticles induced photoelectric current in environmentally-friendly plasmon-sensitized solar cell, Light Sci. Appl. 1 (6) (2012) e14–e14.
[41] B. Wang, X. Zhu, S. Li, M. Chen, N. Liu, H. Yang, M. Ran, H. Lu, Y. Yang, Enhancing the photovoltaic performance of perovskite solar cells using plasmonic Au@Pt@Au core-shell nanoparticles, Nanomaterials (Basel) 9 (9) (2019).
[42] X.-Y. Wang, J.-L. Wang, H. Wang, Improvement of the efficiency and power output of solar cells using nanoparticles and annealing, Sol. Energy 101 (2014) 100–104.
[43] A.R. Warrier, R. Gandhimathi, Surface plasmon resonance induced enhancement of photoluminescence and Raman line intensity in SnS quantum dot-Sn nanoparticle hybrid structure, Methods Appl. Fluoresc. 6 (2018), 035009.
[44] H.-S. Yun, B.-w. Park, Y.C. Choi, J. Im, T.J. Shin, S.I. Seok, Efficient nanostructured TiO_2/SnS heterojunction solar cells, Adv. Energy Mater. 9 (35) (2019), 1901343.
[45] N. Spalatu, J. Hiie, R. Kaupmees, O. Volobujeva, J. Krustok, I.Oja Acik, M. Krunks, Postdeposition processing of SnS thin films and solar cells: prospective strategy to obtain large, sintered, and doped SnS grains by recrystallization in the presence of a metal halide flux, ACS Appl. Mater. Interfaces 11 (19) (2019) 17539–17554.
[46] N. Manh Hung, C.V. Nguyen, V.K. Arepalli, J. Kim, N. Duc Chinh, T.D. Nguyen, D.-B. Seo, E.-T. Kim, C.J. Kim, D.J. Kim, Defect-induced gas-sensing properties of a flexible SnS sensor under UV illumination at room temperature, Sensors 20 (19) (2020) 5701.
[47] W. Albers, C. Haas, H.J. Vink, J.D. Wasscher, Investigations on SnS, J. Appl. Phys. 32 (10) (1961) 2220–2225.
[48] J. Henry, K. Mohanraj, S. Kannan, S. Barathan, G. Sivakumar, Structural and optical properties of SnS nanoparticles and electron-beam-evaporated SnS thin films, J. Exp. Nanosci. 10 (2) (2015) 78–85.
[49] P.M. Nikolic, P. Mihajlovic, B. Lavrencic, Splitting and coupling of lattice modes in the layer compound SnS, J. Phys. C 10 (11) (1977) L289–L292.
[50] F. Ballipinar, A.C. Rastogi, Tin sulfide (SnS) semiconductor photo-absorber thin films for solar cells by vapor phase sulfurization of Sn metallic layers using organic sulfur source, J. Alloys Compd. 728 (2017) 179–188.
[51] S. Sohila, M. Rajalakshmi, C. Ghosh, A.K. Arora, C. Muthamizhchelvan, Optical and Raman scattering studies on SnS nanoparticles, J. Alloys Compd. 509 (19) (2011) 5843–5847.

[52] S. Fateixa, H.I.S. Nogueira, T. Trindade, Hybrid nanostructures for SERS: materials development and chemical detection, Phys. Chem. Chem. Phys. 17 (33) (2015) 21046–21071.
[53] M. Devika, N. Koteeswara Reddy, M. Prashantha, K. Ramesh, S. Venkatramana Reddy, Y.B. Hahn, K.R. Gunasekhar, The physical properties of SnS films grown on lattice-matched and amorphous substrates, Phys. Status Solidi A 207 (8) (2010) 1864–1869.
[54] H.S. Im, Y. Myung, Y.J. Cho, C.H. Kim, H.S. Kim, S.H. Back, C.S. Jung, D.M. Jang, Y.R. Lim, J. Park, J.-P. Ahn, Facile phase and composition tuned synthesis of tin chalcogenide nanocrystals, RSC Adv. 3 (26) (2013) 10349–10354.
[55] W. Guo, Y. Shen, M. Wu, T. Ma, Highly efficient inorganic–organic heterojunction solar cells based on SnS-sensitized spherical TiO_2 electrodes, Chem. Commun. 48 (49) (2012) 6133–6135.
[56] V.R. Minnam Reddy, S. Gedi, C. Park, M. R.W, R.R. K.T, Development of sulphurized SnS thin film solar cells, Curr. Appl. Phys. 15 (5) (2015) 588–598.
[57] S.-I. Son, D. Shin, Y.G. Son, C.S. Son, D.R. Kim, J.H. Park, S. Kim, D. Hwang, P. Song, Effect of working pressure on the properties of RF sputtered SnS thin films and photovoltaic performance of SnS-based solar cells, J. Alloy. Compod. 831 (2020), 154626.
[58] P. Jain, P. Arun, Localized surface plasmon resonance in SnS:Ag nano-composite films, J. Appl. Phys. 115 (20) (2014), 204512.
[59] J. Szeremeta, M. Nyk, M. Samoc, Photocurrent enhancement in polythiophene doped with silver nanoparticles, Opt. Mater. 37 (2014) 688–694.
[60] M. Devika, N.K. Reddy, F. Patolsky, K.R. Gunasekhar, Ohmic contacts to SnS films: selection and estimation of thermal stability, J. Appl. Phys. 104 (12) (2008), 124503.
[61] B. Ghosh, M. Das, P. Banerjee, S. Das, Characteristics of metal/p-SnS Schottky barrier with and without post-deposition annealing, Solid State Sci. 11 (2) (2009) 461–466.